2011 IEEE International Conference on Robotics and Automation
Shanghai International Conference Center
May 9-13, 2011, Shanghai, China

An adaptive knee joint exoskeleton based on biological geometries

Dong-hai Wang, Jiajie Guo, Kok-Meng Lee, *Fellow, IEEE/ASME*, Can-jun Yang, and Hui Yu

Abstract— **This paper presents a dynamic model of a knee joint interacting with a two-link exoskeleton for investigating the effects of different exoskeleton designs on internal joint forces. The closed kinematic chain of the leg and exoskeleton has a significant effect on the joint forces in the knee. A bio-joint model is used to capture this effect by relaxing a commonly made assumption that approximates a knee joint as a perfect engineering pin-joint in exoskeleton design. Based on the knowledge of a knee-joint kinematics, an adaptive knee-joint exoskeleton has been designed by incorporating different kinematic components (such as a pin, slider and cam profile). This design potentially eliminates the negative effects associated with the closed leg/exoskeleton kinematic chain on a human knee. An investigation in the flexion motion of an artificial human knee joint is presented to compare performances of five exoskeleton designs against the case with no exoskeletons. Analytical results that estimate internal forces using the dynamic model (based on the properties of a knee joint) agree well with the experiments. These studies lead to an adaptive mechanism with a slider/cam as an alternative to pin joints for the exoskeleton, and illustrate the application of the model for designing an adaptive mechanism that minimizes internal joint forces due to a human-exoskeleton interaction.**

Index terms: **Bio-joint model, adaptive design, rehabilitation exoskeleton, knee joint internal force**

I. INTRODUCTION

Exoskeletons have been widely studied in mechatronics and robotics for rehabilitating and assisting human body motions. The driven gait orthosis (DGO) [1] provides the patients with therapy and reduces repeated laborious workload for therapists. The Berkeley Lower Extremity Exoskeleton (BLEEX) [2] helps humans carry heavy load on rough terrains using a pair of robotic legs. A powered ankle-foot orthosis [3] is designed for studying gait biomechanics and ankle rehabilitation. A high fidelity four degrees of freedom (DOFs) wrist exoskeleton robot (RiceWrist) is presented in [4] for wrist rehabilitation and training based on kinesthetic feedback. Although the exoskeleton or orthosis can assist or adjust human musculoskeletal system, there can be potential damages and injuries if it is not adaptive to the subject who wears it. To reduce the negative effects from the rigid exoskeleton on human joints, the interaction forces between human and exoskeleton and its effects on human internal joints must be well understood.

Traditional exoskeletons are designed based on simplifying the biological joint (bio-joint) as a simple engineering pin joint. For example, the knee joint in traditional exoskeletons [5] is assumed as a hinge which has only one DOF. However, unlike an engineering joint with a fixed rotation axis, a bio-joint with a non-uniform geometry such as a varying articulating surface, often has a non-constant rotation axis. In fact, the knee joint has flexion and extension in one plane and rotation in another plane [6]. The natural kinematics of the bio-joint must be considered when designing an exoskeleton to assist it. In [7], a three-dimensional analytical model taking into account the knee-joint surface geometry is presented. For standardization in a clinical joint coordination system, the knee joint is described with six DOFs in [8].

In this paper, the flexion of an artificial human knee joint is investigated for comparing the performances of different exoskeleton designs against the case without exoskeleton. The human knee instrumented with a two-link mechanism forms a closed-kinematic loop. It tends to create a residual force if the DOFs of the exoskeleton are insufficient to compromise with that of human joint to align their motion axes [9]-[10]. Considering the knee joint with two DOFs (rotation and translation), the closed kinematic chain experiences a singularity when the knee is fully extended, and thus introducing impulses into the internal joint forces [11], which, unlike the case of an open kinematic chain (such as human walking with no exoskeleton) experiencing no impulse within the joint. Exoskeleton designs with insufficient knowledge of joint motions can disturb and even damage human joints; thus, the bio-joint kinematics should be fully accounted for in exoskeleton designs.

Numerous methods have been proposed to measure the internal human joint forces, and can be broadly classified into two major categories; namely, simulation and experiment. While experimental techniques have helped determine loading in the hip [12], spine [13] and knee [14], they generally involve instrumented prostheses or implant in-vivo. Besides these in-vivo measurements, inverse dynamic models of human lower extremity have also been developed for simulating the musculoskeletal loads in daily activities [15]-[17]. Simulation methods are more realizable as

This work was supported in part by the National Science and Technology Ministry under Grant 2009BAI71B03, the Program for New Century Excellent Talents in University under Grant NCET-07-0756, the Fundamental Research Funds for the Central Universities under Grant 2009QNA4003.

Dong-hai Wang, Prof. Can-jun Yang and Hui Yu are with the Institute of Mechatronic Control Engineering, Zhejiang University, 310027 P. R. China

Jiajie Guo and Prof. K.-M. Lee and are with the George W. Woodruff School of Mechanical Engineering, Georgia Institute of Technology, Atlanta, GA 30332-0405, USA Prof. K.-M. Lee (email: kokmeng.lee@me.gatech.edu). is visiting Pao Yu-Kong Chair Professor at the Zhejiang University.

compared with dangerous operative procedures.

This paper begins with extending the kinematic and dynamic models formulated in [11] for a closed-kinematic chain mechanism consisting of a human knee joint and an exoskeleton, which are then employed to estimate the effects of exoskeleton on the internal forces within a human knee. Several kinematic configurations are analyzed leading to the design concept of an adaptive exoskeleton. The validity of the models has been examined by comparing simulated results against those obtained experimentally on an existing lower-extremity rehabilitation exoskeleton (LERE) [18], which has been modified to accommodate natural motion of a typical human knee.

II. Theory

A. Knee joint kinematics and dynamics

Figure 1(a) shows a human knee joint flexing with an exoskeleton attached at E on the lower leg while the upper leg is held stationary, where a lumped-parameter approach in a polar coordinate (r, θ) is used to describe forces involved in the analysis. The lower leg is modeled as a mass centered at O and is subjected to gravity. As illustrated in Fig. 1(b), C is the current contact point between the femur and the tibia; and C_i is the initial contact point on the femur. Since the femur is fixed in this study, C_i is a fixed point in space. In Fig. 1, the reference (defined as the flexion angle θ = 0°) is along the longitudinal axis of the upper leg; the distance r is measured from C_i to O; and (f_r, f_θ) and τ_a are the resultant forces and torque exerted by the femur and surrounding tissues (muscle and ligament) on the tibia in e_r and e_θ directions and about the normal to the r-θ plane at C_i, respectively.

The exoskeleton consists of two links connected by a pin joint which is assumed to coincide with C_i. The lower-link motion of the exoskeleton is characterized by its mass center O_e using coordinates (r_e, ϕ) as shown in Fig. 1(b) where θ_E is the misalignment angle between the exoskeleton and the axis of the lower leg. As will be shown, θ_E is small (within 10°). As illustrated in Fig. 1(a), the exoskeleton exerts f_{er} and $f_{e\theta}$ forces at the attaching point E on the lower leg in e_r and e_θ directions respectively in addition to the torques due to its gravitation τ_g and actuation τ_E.

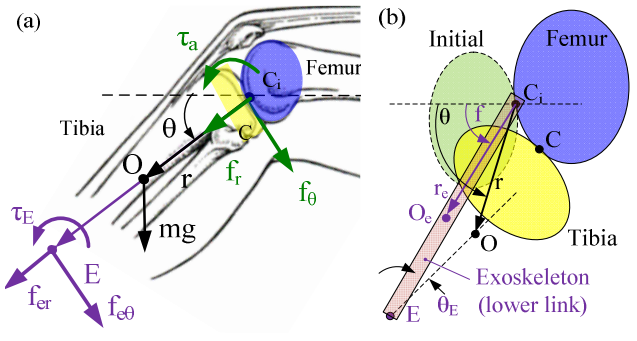

(a) Coordinates and forces (b) Illustration of kinematics

Fig. 1. Knee joint rotation

A relatively complete bio-joint model has been formulated in [11] for simulating the human knee-joint rotation:

$$\dot{r} = \omega \frac{dr}{d\theta}, \ddot{r} = \dot{\omega}\frac{dr}{d\theta} + \omega^2 \frac{d^2 r}{d\theta^2} \qquad (1a,b)$$

where $\omega = d\theta/dt$. For a given θ trajectory, the r, r_e and ϕ motions of the combined human-exoskeleton system can be readily calculated [11]. The interest here is to investigate the effects of different exoskeleton designs on the joint forces/torques, which can be computed from the equations of motion describing the dynamics of the lower leg in (2) and the lower link of the exoskeleton in (3):

$$m(\ddot{r} - r\dot{\theta}^2) = mg\sin\theta + f_r + f_{er}\cos(\phi-\theta) - f_{e\theta}\sin(\phi-\theta) \qquad (2a)$$

$$m(2\dot{r}\dot{\theta} + r\ddot{\theta}) = mg\cos\theta + f_\theta + f_{er}\sin(\phi-\theta) + f_{e\theta}\cos(\phi-\theta) \qquad (2b)$$

$$J\ddot{\theta} + 2mr\dot{r}\dot{\theta} = \tau_g + \tau_a + \tau_E + f_{e\theta}r_E \qquad (2c)$$

$$J_e\ddot{\phi} + 2m_e r_e \dot{r}_e\dot{\phi} = \tau_{ge} - f_{e\theta}r_E - \tau_E \qquad (3)$$

where m and J are the mass and moment of inertia of the lower leg; r_E is the distance from C_i to E; m_e and J_e are the mass and moment of inertia of the exoskeleton; and f_{ge} and τ_{ge} are the force and torque due to gravity respectively. In (2c) and (3), the torques and moments of inertia are computed with respect to C_i. For a given exoskeleton design,

$$f_{er} = -k_r(r_E - r_{E(0)}) - \text{sign}(\dot{r}_E)\mu f_{e\theta} \qquad (4a)$$

$$\tau_E = k_\theta \theta_E \qquad (4b)$$

$$\theta_E = \cos^{-1}\left[\left(\mathbf{r_E} \bullet \overline{OE}\right)/\left(r_E|OE|\right)\right] \qquad (4c)$$

where $r_{E(0)}$ is the initial value of r_E; the stiffness k_r and k_θ models the compliance at E; and μ is the friction coefficient.

B. Designs of the knee joint exoskeleton

The effect of the exoskeleton designs on the internal joint forces (f_r, f_θ) has been investigated numerically, where a human knee-joint flexing actively and freely without any exoskeleton serves as a basis for comparison. The upper leg and link are held stationary, while the lower link is connected via a pin joint or actuated through a cam mechanism located at the same position as C_i. Five design configurations (summarized in Table 1) are considered:

DC1 (Pin and fixed end):

The link is connected by engineering pin-joint to the fixed brace; r_e is a constant in (3). However, because rigid links cannot adapt to the changing distance r, the attachment E is subjected to compression/extension and torsion.

DC2 (Pin and slider):

The link is allowed to slide with respect to the leg brace to accommodate for the knee-joint translational motion in e_r direction. This relaxes the compression at E; r_E=$r_{E(0)}$ or k_r = 0.

DC3 (Cam and slider):

To account for the biological geometry of the knee joint, the hinge in DC2 is replaced by a grooved cam which allows the distance r_e to vary with the knee-joint motion. Thus r_e is no longer a constant but changes with the cam profile.

DC4 (Pin and pinned slider):

The hinge in DC2 is allowed to slide and rotate to account

for the misalignment θ_E between the link and leg; $k_\theta = 0$ because a hinge cannot transmit torques.

DC5 (Cam and pinned slider):

The hinge in DC3 is allowed to slide and rotate. Combined with a grooved cam, this design can accommodate both the changing distance r and the misalignment θ_E.

Table 1: Specifications of exoskeleton designs.

No exoskeleton  None	DC 1 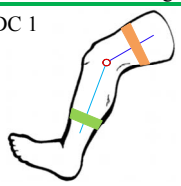 constant r_E $k_r \neq 0$ and $k_\theta \neq 0$	DC 2 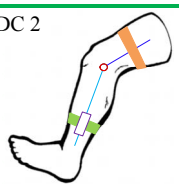 constant r_E $k_r = 0$ and $k_\theta \neq 0$
DC 3 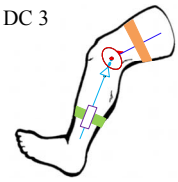 cam profiled r_E $k_r = 0$ and $k_\theta \neq 0$	DC 4 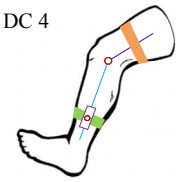 constant r_E $k_r = k_\theta = 0$	DC 5 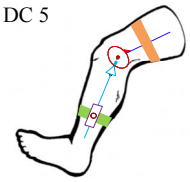 cam profiled r_E $k_r = k_\theta = 0$

To accommodate the human knee-joint motion, a cam profile is designed based on the following considerations:

a. Both the lower leg and link rotate in parallel, $\theta_E = 0$.

b. It is designed to follow the changing distance r of the tibia mass-center from the initial contact point C_i, which is available in [11]:

$$r(\theta) = 1.078\theta^4 - 11.184\theta^3 + 26.542\theta^2 - 0.825\theta + 263.59 \quad (5)$$

c. The cam can stably support the weight of both human and exoskeleton when standing. This implies that the contact area on the cam profile should be flat at $\theta = 0°$.

The design began with a preliminary cam profile to eliminate the constant term in (5). The motion that the lower leg and link flex in parallel can be represented by a line passing through the origin with the instantaneous contact point moving on the red solid line in the polar coordinate in Fig. 2. This cam profile, however, cannot support the human/exoskeleton as the slope of the curve is negative near $\theta = 0°$ around which the upper link will slip from a high potential energy state while the human is standing. Thus, the cam profile is modified by adding a sinusoidal term as shown in (6a, b) and in Fig. 2 (green dash-dot line):

$$\tilde{r}(\theta) = 1.078\theta^4 - 11.184\theta^3 + 26.542\theta^2 - 0.825\theta + s \quad (6a)$$

$$\text{where } s = 20\cos(\theta + 0.0873) \quad (6b)$$

A slider is added at the end interaction point to compensate for the influence of the sinusoidal term, and the slight difference due to human biological geometrical variation. This mathematically derived profile can be easily machined.

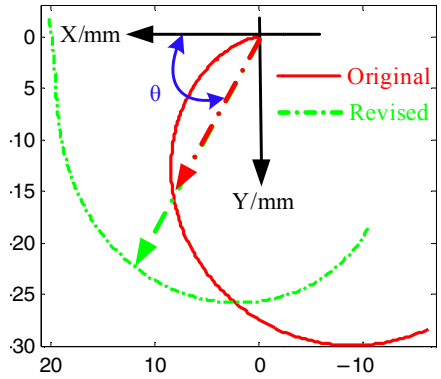

Fig. 2. Designs of cam profiles (X axis is along the axis of the femur)

III. Experimental Setup

Figure 3 shows the experimental test-bed built upon an existing two-link LERE [18] for investigating the effect of the exoskeleton on the internal forces in the artificial knee joint as the tibia and lower-link rotate with respect to the fixed femur and upper-link. An artificial model (3B Scientistic functional knee joint, which consists of portions of femur, tibia and fibula; also includes meniscus, patella with quadriceps tendon and joint ligaments), was used to simulate the mechanics of the knee joint in experiments. The artificial joint is passive (imitating a patient sitting with lower leg flexion from full extension), and rotated with the exoskeleton lower-link actuated by a DC motor.

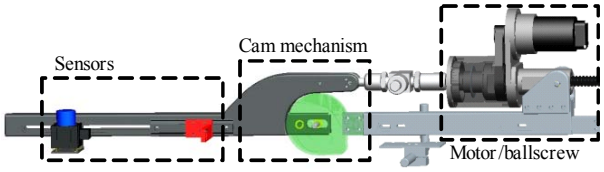

(a) CAD model illustrating the lower-link of the LERE

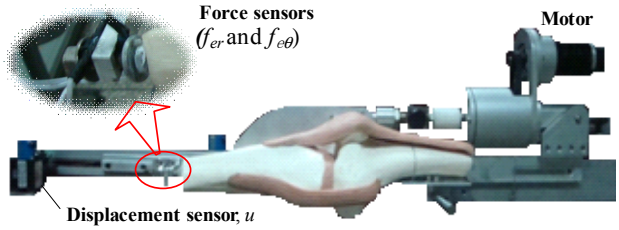

(b) Artificial knee joint attached on the lower-link

Fig. 3. Experimental test-bed for displacement and force measurements

The LERE (with θ limited to 70°) was modified so that the five different configurations can be compared. As shown in Fig. 3, force sensors (Honeywell piezoresistive FSS) are installed at the end of the tibia measuring the forces (f_{er} and $f_{e\theta}$) between the tibia and exoskeleton. In addition, a displacement sensor (ASM cable-driven potentiometer CLMZ3) is fixed on the exoskeleton lower-link such that its measuring terminal (displacement u) moves with the end of the tibia along e_r direction. Since the tibia is rigid,

$$r = r_i + u \quad (7)$$

where r_i is the initial r value when the knee is fully extended. The actuator/sensors specifications are given in Table 2.

Figure 4 shows the CAD model of the adaptive

exoskeleton, where two cam slots are fixed on its upper-link. The lower link rotates as the roller follows the cam profile (designed to capture the human knee joint geometry) while allowing the pin (with a nylon sleeve) to slide for accommodating the motion of the knee axis. A passive joint is added to compensate for the misalignment between lower leg and exoskeleton link [10]. Different configurations can be investigated by engaging/disengaging some kinematic pairs.

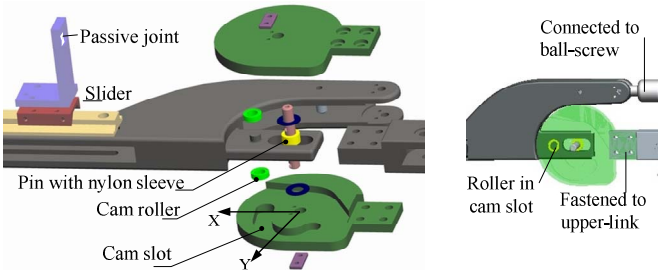

(a) Exploded view (b) Side view

Fig. 4. Cam mechanism CAD model (X-Y coordinates are defined in Fig. 2)

Table 2: Experimental setup specifications

DC servomotor (Nominal values)	Voltage	Current	Torque
	24 V	5.77 A	170 mNm
	Speed	Torque constant	Rotor inertia
	6930 rpm	30.2 mNm/A	138 gcm^2
Displacement sensor	Range	Potentiometer	Accuracy
	250 mm	1 KΩ	0.035%
Force sensor	Range	Sensitivity	Linearity
	1500 g	0.12 mV/g	±1.5 %
	Measurements , H×W×D: 3.25mm×9.14mm×3.81mm		

IV. RESULTS AND DISCUSSION

Two sets of results are discussed. The 1st set compares the measured mass-center displacement of the artificial lower-leg from C_i against results simulated using the scaled anatomically-based model. The 2nd set studies the effects of different configurations on the internal forces in the knee joint. The knee joint geometry is modeled by fitting the artificial knee with two ellipses scaled from an anatomically based knee joint model [11] by a factor of 0.77. The specifications of the lower leg and link are listed in Table 3, where J is with respect to C_i; and the cam profile origin is at the initial state (fully extended knee). For simulation purposes, the cam/slider pair is assumed frictionless ($\mu = 0$), and the attachment is elastic (constant k_r and k_θ).

Table 3: Specifications of human and exoskeleton lower legs

	Length (mm)	Mass (kg)	Moment of inertia J (kg·m^2)
Human	157.5	0.164	5.68×10^{-4}
DC1, 2, 4	360	0.4215	1.214×10^{-2}
DC3, 5	395	0.3906	1.489×10^{-2}
	r_{maj} (mm)	r_{min} (mm)	Attachments
Femur	25.85	17.7	k_r = 4000 N/m
Tibia	22.2	14.5	k_θ = 15 Nm/radian

The motor-driven link that flexes the knee joint follows a trapezoidal-velocity trajectory from a static initial state:

Constant acceleration: $\theta = -5°$ to $\theta = 6.5°$ for 1.6s

Constant velocity: $\theta = 6.5°$ to $\theta = 57.5°$ for 3.5s

Constant deceleration to the static state $\theta = 69°$ for 1.6s.

A. Comparison of the displacement r

Figure 5 shows snapshots of the knee rotation at θ = 0°, 60° and 120° illustrating the kinematic relationship between the lower leg and the lower link of an exoskeleton, where the misalignment angle $\angle EC_iO$ is given by

$$\theta - \phi = \cos^{-1}\left[(\mathbf{r} \bullet \mathbf{r}_E)/(rr_E)\right] \quad (8)$$

The simulated and measured r displacements computed from (9a, b) and their time-derivatives are compared in Fig. 6.

$$r_{sim}(\theta) = 0.83\theta^4 - 8.61\theta^3 + 20.44\theta^2 - 0.64\theta + 54.48 \quad (9a)$$

$$r_{\exp}(\theta) = -8.01\theta^4 + 14.48\theta^3 + 4.59\theta^2 - 1.45\theta + 56.48 \quad (9b)$$

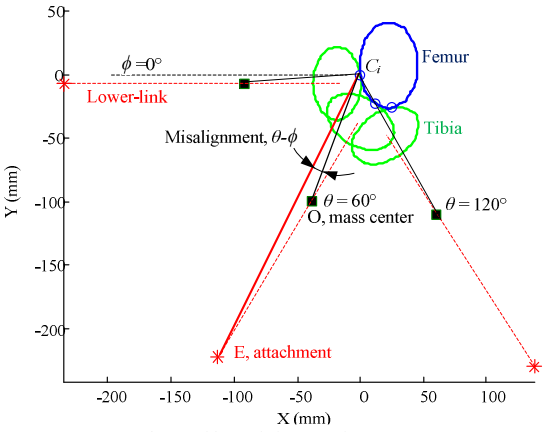

(a) Snapshots of knee joint rotation at θ=0°, 60°, 120°.
(o: Current contact points. □: Mass-center O. *: Attachment E)

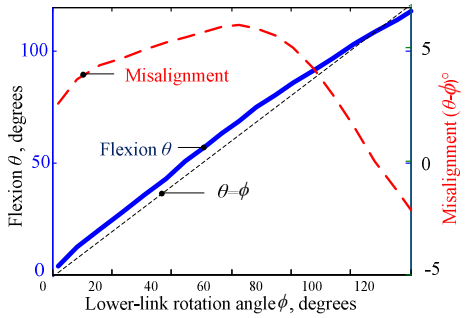

(b) Misalignment between lower leg and link

Fig. 5 Kinematic relationship between link rotation and flexion

Simulated $r(\theta)$ results, in general, are consistent with experimental data. Some deviations observed near initial flexions in Fig. 6(a) could be due to two reasons: i) Simulations results are based on a knee geometry scaled from a nominal model without considering the specific details f of the artificial knee joint. ii) The offset between the upper leg and lower link results in a misalignment (within 10° for $\theta \in [-5°, 120°]$). To account for the offset, the simulation assumes $\theta = -5°$ when $\phi = 0°$ and the link rotates about C_i. The $r(\theta)$ discrepancy has been the primary cause of the errors in the time-derivatives in Fig. 6(b), which are derived from the polynomial fits of (9). The sudden jumps at $\theta = 6.5°$ and 57.5° are due to the step change in acceleration defined in the trapezoidal velocity trajectory.

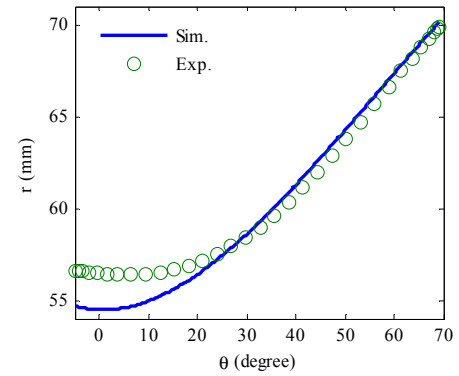

(a) Displacement

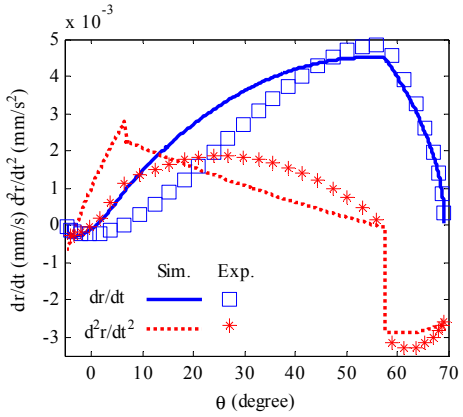

(b) 1st and 2nd time-derivatives of r

Fig. 6. Comparison between simulation and experiment

B. *Effect of exoskeleton on knee joint internal forces*

Simulation and experimental results of the five design configurations are compared in Fig. 7 against the case without exoskeleton to investigate the effects of exoskeletons on human knee joint internal forces. Noting that f_r represents the force from the tissues if tensile force dominates or otherwise from bones which primarily provide compressive forces, some observations are summarized as follows:

- Without exoskeleton, the leg is a freely moving open-chain mechanism with low internal forces experienced in the knee (Fig. 7a). Due to directional components of the lower-leg gravity, f_r is negative (tensile) with increasing magnitude while f_θ decreases in magnitude.
- With the one DOF DC1 (Fig. 7b), the combined leg and exoskeleton forms an over-constrained closed-chain mechanism. Except near zero flexion where some discrepancies due to the error in Fig. 6 (a) are observed, simulation and experiments closely agree, which show a significantly large compressive f_r between femur and tibia, increasing with θ. The discrepancy in f_θ at large flexions suggests a violation in the assumption that the attachment at E is linear elastic in simulation. However, simulations with an accurate k_θ could offer more realistic f_θ estimation than that with a rigid attachment (as in the experimental setup) in practice where the attachment between the exoskeleton and leg likely incorporates some compliance (human skin) that would relax some internal forces but at the expense of uncomfortable slip.
- The slider in DC2 and DC3, which offers a translational DOF along the e_r direction, greatly reduces the internal forces in the knee joint, particularly a remarkable decrease in the magnitude of f_r. As observed in the experimental results, because the cam profile was designed to adapt to the changing distance r but not the misalignment θ_E at E, some compressive f_r can still be seen in certain flexion angles. In addition, the f_θ experimental data in DC2 and DC3 are significantly higher than that in the case of no exoskeleton.
- In DC4 and DC5, a pin joint is incorporated with the slider at E for compensating the misalignment θ_E that gives rise to torsion (between the lower-leg and lower-link) and increases in $f_{e\theta}$ that contributes to the friction in the slider and thus increases in f_r. This added pin joint (which sets free the torque) results in smaller f_r and f_θ as compared to DC2 and DC3.
- Theoretically, a cam profile shaped to perfectly fix the specific knee motions would be ideal. However, such perfectly fixed model could be a daunting task (if not impossible). Some insights into the effect of the cam profile on the internal forces of a knee joint (that is 25% smaller than the nominal model from which the cam is designed) can be gained by comparing the experimental results obtained from the 2DOF DC3 and the 3DOF DC5:
  a) When the over-sized cam profile is used on an over-constrained system, the f_r variation (both compressive and tensile) is significantly larger than that in DC2 (without cam) as compared in Fig. 7(d).
  b) The same cam profile when used in DC5 results in smaller f_r and f_θ magnitudes than those of all four other configurations. It is expected that compressive f_r near zero flexion can be minimized with some fine-tuning.
- Except for DC1, simulated f_θ agrees well with data obtained experimentally. Experimental results from all five configurations show that f_θ exhibits an inverse trend against the case with no exoskeleton; this is primarily because the exoskeleton exerts its own weight/actuation on the lower leg through the attachment E. The large discrepancies between simulated and experimental f_r suggest that non-linear effects such as meniscus compliance between femur and tibia and friction in the slider and cam mechanisms cannot be neglected in the simulation.

V. Conclusions

The kinetics of a human lower leg-exoskeleton system has been formulated to investigate the effects of different design configurations on the joint internal forces. By capturing the non-uniform geometry of a natural knee joint using the bio-joint model, several factors associated with the changing rotation radius and the misalignment between the lower leg and exoskeleton-link have been analyzed theoretically and

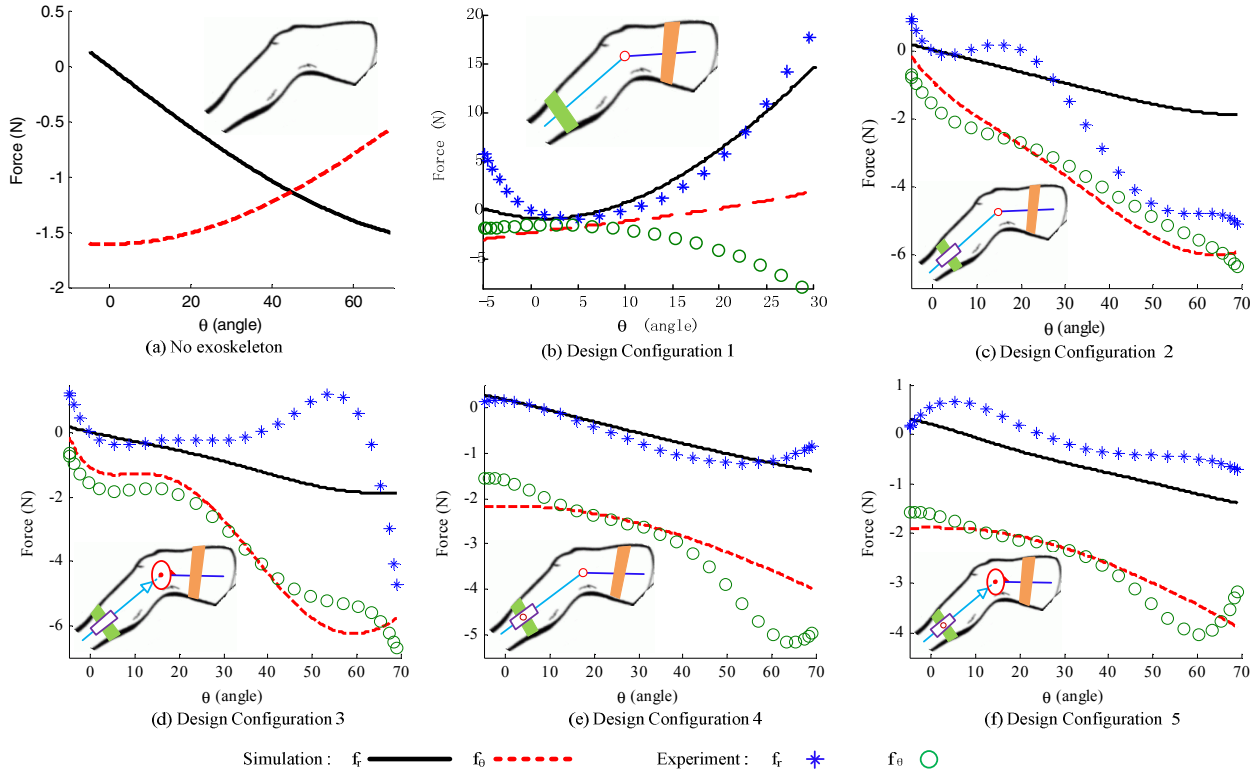

Fig. 7. Effects of different design configurations (Table 1) on human knee joint (Insets with background image from the Internet public domain [19]).

experimentally using an artificial human knee-joint. This is performed by comparing the dynamic performances of five different exoskeleton configurations against the case with no exoskeleton. These exoskeleton designs are presented by combinations of different kinematic components, such as a pin, slider and cam. The effects of oversized cam profile (scaled from an anatomically-based knee-joint model to adapt an exoskeleton to the natural joint motions) on the internal forces have been investigated. Experimental findings suggest that incorporating an appropriately scaled slider/cam can effectively minimize internal joint forces from the human-exoskeleton interaction.

REFERENCES

[1] G. Colombo, M. Joerg, R. Schreier, and V. Dietz, "Treadmill training of paraplegic patients using a robotic orthosis," *J. Rehabil. Res. Develop.*, V. 37 (6), pp. 693-700, 2000.

[2] A. Chu, H. Kazerooni, and A. Zoss, "On the biomimetic design of the berkeley lower extremity exoskeleton (BLEEX)," *in Proc. IEEE Int. Conf. Robot. Automation*, Barcelona, pp. 4345–4352, 2005.

[3] D. P. Ferris, K. E. Gordon, G. S. Sawicki, and A. Peethambaran, "An improved powered ankle-foot orthosis using proportional myoelectric control," *Gait and Posture*, V. 23 (4), pp. 425-428, 2006.

[4] A. Gupta, M. K. O'Malley, V. Patoglu, and C. Burgar, "Design, control and performance of ricewrist: a force feedback wrist exoskeleton for rehabilitation and training," *Int. J. Robot. Res.*, V. 27 (2), pp. 233–251, 2008.

[5] A. Zoss, H. Kazerooni and A. Chu, "On the mechanical design of the Berkeley lower extremity exoskeleton (BLEEX)," *Proc. IEEE/RSJ Int. Conf. Intelligent Robots and Syst.*, Edmonton, pp. 3465 – 3472, 2005.

[6] http://ovrt.nist.gov/projects/vrml/h-anim/jointInfo.html

[7] J. Wismans, F. Veldpaus, J. Janssen, A. Huson and P. Struben, "A three-dimensional mathematical model of the knee-joint," *J. Biomechanics*, V. 13 (8), pp. 677-679, 681-685, 1980.

[8] G. Wu, and P. R. Cavanagh, "ISB recommendations for standardization in the reporting of kinematic data," *J. Biomechanics*, V. 28 (10), pp. 1257-1261, 1995.

[9] A. H. A. Stienen, E. E. G. Hekman, F. C. T. van der Helm, and H. van der Kooij, "Self-aligning exoskeleton axes through decoupling of joint rotations and translations," *IEEE Trans. Robotics*, V. 25 (3), pp. 628-633, 2009.

[10] A. Schiele and F. C. T. van der Helm, "Kinematic design to improve ergonomics in human machine interaction," *IEEE Trans. Neural Syst. Rehabil. Eng.*, V. 14 (4), pp. 456-469, 2006.

[11] K.-M. Lee, and J. Guo, "Kinematic and dynamic analysis of an anatomically based knee joint," *J. Biomechanics*, V. 43 (7), pp. 1231-1236, 2010.

[12] F. Graichen, G. Bergmann, and A. Rohlmann, "Hip endoprosthesis for in vivo measurement of joint force and temperature," *J. Biomechanics*, V. 32 (10), pp. 1113-1117, 1999.

[13] A. Rohlmann, G. Bergmann, and F. Graichen, "Loads on internal spinal fixators measured in different body positions," *Eur. Spine J.*, V. 8, pp. 354-359, 1999.

[14] H. J. Kim, J. W. Fernandez, M. Akbarshahi, J. P. Walter, B. J. Fregly, and M. G. Pandy, "Evaluation of predicted knee-joint muscle forces during gait using an instrumented knee implant," *J. Orthopaedic Research*, V. 27 (10), pp. 1326-1331, 2009.

[15] T. Wehner, L. Claes, and U. Simon, "Internal loads in the human tibia during gait," *Clin. Biomechanics*, V. 24 （3）, pp. 299-302, 2009.

[16] W. R. Taylor, M. O. Heller, G. Bergmann, and G. N. Duda, "Tibio-femoral loading during human gait and stair climbing," *J. Orthopaedic Research*, V. 22 (3), pp. 625-632, 2004.

[17] A. Thambyah, B. P. Pereira, and U. Wyss, "Estimation of bone-on-bone contact forces in the tibiofemoral joint during walking," *The Knee*, V. 12 (5), pp. 383-388, 2005.

[18] J.F. Zhang, Y.M. Dong, C.J. Yang, Y. Geng, Y. Chen and Y. Yang, "5-Link model based gait trajectory adaption control strategies of the gait rehabilitation exoskeleton for post-stroke patients," *Mechatronic*s, 20(3), pp. 368-376, 2010.

[19] http://www.123coloring.com/coloringpages/nature/human%20body/images/corpshumain_002.gif